BEFIB2012 – Fibre reinforced concrete
Joaquim Barros et al. (Eds)

DESIGN-CURVES OF STRAIN SOFTENING AND STRAIN HARDENING FIBRE REINFORCED CONCRETE ELEMENTS SUBJECTED TO AXIAL LOAD AND BENDING MOMENTS

Rajendra Varma*, Joaquim A.O. Barros* and José M. Sena-cruz*

* ISISE, Dep. Civil Eng., School Eng., University of Minho
Campus de Azurém 4800-058 Guimarães, Portugal
e-mail: rajendra@civil.uminho.pt, barros@civil.uminho.pt, jsena@civil.uminho.pt, web page: www.isise.net

Keywords: Fibre reinforced concrete, design curves, bending moment, axial load, strain hardening, strain softening.

Summary: *Several structural components made by fibre reinforced concrete (FRC) are submitted to axial load and bending moments. In some cases fibres cannot replace completely the conventional reinforcement, even if strain hardening FRC is used; therefore the optimization of the reinforcement solution for these elements depends on the post-cracking behaviour of the FRC, as well as the percentage of conventional reinforcement to replace. To fully exploit the FRC capabilities, the development of a suitable, comprehensive and design-oriented model of its tensile response is of the utmost importance. To provide a practical tool for the pre-design of FRC-structural-elements subjected to axial load and bending moments, design curves were generated using a computational program capable of simulating the main features of the tensile and compressive behaviour of strain softening and strain hardening FRC's, and steel bars. The post-cracking tensile behaviour of the FRC is characterized by two parameters that define its residual strength ratio (α) and its corresponding tensile strain ratio (β). To generate these curves, a parametric study is carried out based on the tensile parameters α and β and considering distinct mechanical reinforcement ratios, from 0 to 1 with a step of 0.2. For every reinforcement ratio, four distinct cases in terms of β are considered; additionally, for every case of β, α is divided from strain hardening to strain softening in five distinct residual strength classes. By sequentially varying α and β, the bending capacity of a section is evaluated to provide a design perspective of the effect of ductility and strength. The model used in this study is described, the design curves are presented and analyzed and some practical design examples are provided.*

1 INTRODUCTION

Romualdi and Mandel [1, 2] proposed for the first time the use of dispersed steel fibres for the reinforcement of concrete elements. Later various other researchers [3-7] have used different types of fibres as dispersed reinforcement. The main aim of using these fibres was to improve the resistance to cracking and crack propagation, as the dispersed fibres are able to hold the concrete matrix together even after extensive cracking. This additional v-μ of concrete increases the post cracking energy absorption capacity. Most of the studies [8-11] conducted during the 70's highlight the increase in terms of energy absorption capacity that strain softening FRC can provide. The strain hardening behaviour in tension was reported, for the first time, by Kasperkiewickz [12]. Naaman and Shah [13] reported inelastic response with multiple cracking and ductile failure during their experiments, which was later, correlated to strain hardening behaviour of this cement composite. In 2005, Naaman and Reinhardt [14] proposed the classification of Fibre Reinforced Concrete (FRC) based on its tensile behaviour assessed from unnotched tensile specimens: it is classified as strain softening FRC (SSFRC) if after crack initiation the stress decreases with the increase of the strain; strain hardening FRC (SHFRC) presents a continuous increase of tensile stress after crack initiation up to its tensile

failure that occurs for a strain level that in general exceeds 1% with the formation of a diffuse crack pattern.

In last decades, several researchers have determined the mechanical tensile properties of FRC. However, despite the important advances on the material characterization, still there is a lack of suitable design methods for FRC. Hence proper description and improvement of design guidelines are needed ([15-16]) so that design and analysis can be conducted reliably. To exploit the FRC capabilities, in the present work a parametric study is presented on use of FRC as partial replacement of reinforcing steel in design of elements submitted to axial force and bending moment.

The paper starts with a brief description of the material constitutive laws adopted in the numerical model for the simulation of the behaviour of the intervening materials. The residual strength ratio (α) and residual tensile strain ratio (β) of FRC (see Figure 1) are the most prominent features of the post-cracking tensile behaviour, which affects the moment carrying capacity of section. For distinct mechanical steel reinforcement ratios (ω), starting from 0 up to 1 with increments of 0.2, a set of v-μ curves are determined, taking in account the combinations of possible ductile behaviour and residual tensile strength of FRC. Finally, the performance of FRC is appraised by a set of design examples where FRC is used to replace conventional longitudinal reinforcement.

2 CONSTITUTIVE LAWS

The envelope curves used to simulate the tensile and compressive behaviour of steel, and the compressive behaviour of concrete is described elsewhere [17]. The tension envelope of FRC is simulated by the stress-strain diagram composed by multi-linear branches represented in Fig. 1, as proposed by Soranakom and Mobasher [18]. The first branch (OA, designated Zone I) simulates the linear-elastic behaviour of FRC up to crack initiation (ε_{ctc}, f_{ctc}). After crack initiation, a SSFRC presents a softening phase characterized by the branch AB´, while a SHFRC shows a hardening phase modelled by the branch AB. This phase (named Zone II) ends at a point characterized by (ε_{ctr}, f_{ctr}). The last phase (BC in case of SHFRC, and B´C´ for SSFRC, designated Zone III) is defined by a constant tensile stress up to the ultimate strain (ε_{ctu}). Zone I is characterized by the initial FRC Young's modulus and ends at the strain for crack initiation (ε_{ctc}) when the stress at crack initiation is installed (f_{ctc}). In zone II the SHFRC exhibits an increase of the tensile stress with the tensile strain due to the formation of multiple cracks, while SSFRC presents a decrease of the tensile stress with the tensile strain due to the formation of one macro-crack. By setting post cracking modulus (E_{cr}) to either a negative or a positive value, strain softening and strain hardening response can be simulated, respectively. Zone III is characterized by a constant stress up to a strain limit above which it is assumed that fibres cannot transfer the residual tensile stresses anymore, so the tensile capacity becomes null. The ratio between this residual stress (f_{ctr}) and f_{ctc} is represented by α, and the ratio between the strain at the initiation of Zone III, ε_{ctr}, and ε_{ctc} is designated by β.

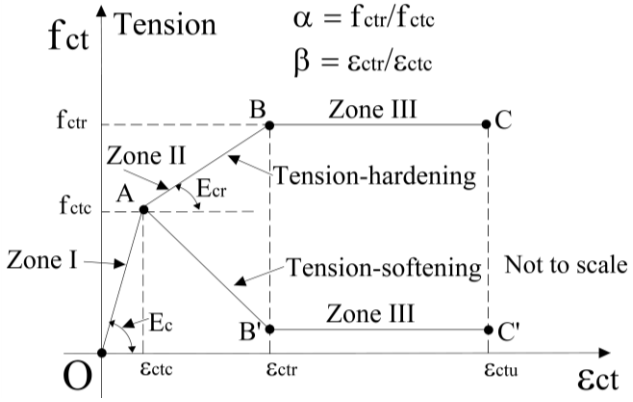

Figure 1: Schematic diagram showing concrete tensile envelope.

The stress-strain relationships for tension envelope are illustrated as:

$$f_{ct} = E_c\ \varepsilon_{ct} \text{ for } 0 \le \varepsilon_{ct} < \varepsilon_{ctc} \tag{1a}$$

$$f_{ct} = E_c\ \varepsilon_{ctc} + E_{cr}(\varepsilon_{ct} - \varepsilon_{ctc}) \text{ for } \varepsilon_{ctc} \le \varepsilon_{ct} < \varepsilon_{ctr} \tag{1b}$$

$$f_{ct} = \alpha\ f_{ctc} \text{ for } \varepsilon_{ctr} \le \varepsilon_{ct} < \varepsilon_{ctu} \tag{1c}$$

$$f_{ct} = 0 \text{ for } \varepsilon_{ct} \ge \varepsilon_{ctu} \tag{1d}$$

3 NUMERICAL MODEL

The moment-curvature diagrams for the cross sections were generated using DOCROS, which is a software developed in University of Minho for Design Of CROss-Section. This model assumes that a plane section remains plane after deformation and bond between materials is perfect. The section is divided in horizontal layers, and the thickness and width of each layer is user-defined and depend on the cross-section geometry (Figure 2). DOCROS can analyze sections of irregular shape and size, composed of different types of materials subjected to an axial force and variable curvature. Composite layers are used when more than one material exist at same depth of the cross section. Each layer can have an initial non-null stress in order to simulate a pre-stress effect. The software can also analyze sections that have layers with distinct construction phases, such as in the case of retrofitting, where strengthening materials are active in later phases. DOCROS has a wide database of constitutive laws for the simulation of monotonic and cyclic behavior of cement based materials, polymer based materials and steel bars. Any layer can be assumed as control layer for which predefined incremental strain is assigned. Assuming the predefined strain of control layer, curvature (χ) of the cross-section is estimated iteratively, assuming the linear strain profile along z-axis [19]. The new constitutive model for modeling the tensile behavior of SS- and SHFRC was implemented in DOCROS.

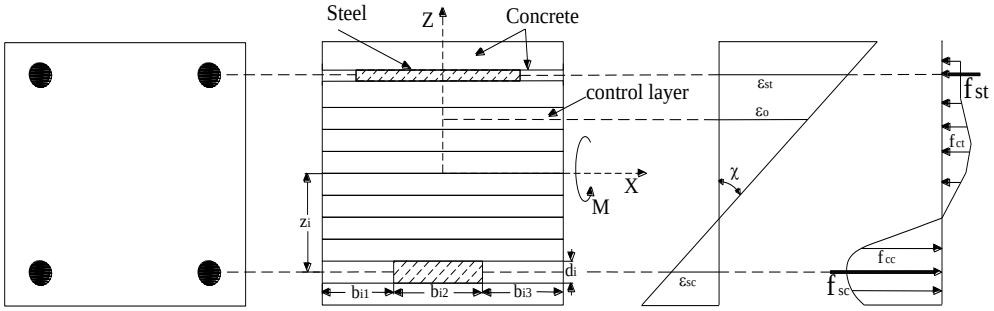

Figure 2: Discretization of a typical section in DOCROS.

The constitutive laws are used to calculate the stresses corresponding to the strains in the layers. The equilibrium of the cross section in terms of force and bending moment is attained by imposing:

$$N = \sum_{i=1}^{n}\left(\sum_{j=1}^{m}\sigma_{ij}d_i b_{ij}\right) \tag{2a}$$

$$M = \sum_{i=1}^{n}\left(\sum_{j=1}^{m}\sigma_{ij}d_i b_{ij} z_i d_i\right) \tag{2b}$$

where N and M are axial load and bending moment, respectively, and n is the number of layers along z-axis. If a composite layer exists at z_i position (see Figure 2), σ_{ij} and b_{ij} represent the stress and the width of layer situated at i^{th} position along z-axis and j^{th} location along x-axis, respectively. In this case m represents the total number of layers along x-axis at i^{th} position, and d_i is the thickness of i^{th} layer. The stress and strain are taken as positive for tension and negative for compression. The algorithm to obtain the M-χ relationship is described in detail elsewhere [19].

4 DESIGN GRAPHS

Symmetrically reinforced cross-section of 200 mm width (b) by 400 mm height (h) with a concrete cover (c) of 20 mm (the bending moment mobilizes the larger moment of inertia of the cross section) was used to develop design curves by varying ω, α and β sequentially. Each design curve is designated by ω***i***α***j***β***k***, where ***i***, ***j*** and ***k*** represent values of ω, α and β, respectively**.** The mechanical steel reinforcement ratio is varied from 0 to 1 with an increment of 0.2 and is calculated as:

$$\omega = A_s f_{sy} / bdf_{ccp} \tag{3}$$

where A_s is the total area of steel reinforcement in the section, f_{sy} and f_{ccp} are yielding stress of steel and the compressive strength of the concrete respectively and; b and d represent the width and effective depth of the section (d=h-c), respectively. As it is assumed that the residual strength can vary from negligible value to a maximum of twice the first cracking strength, hence ***j*** can vary from 0 to 2 with a step of 0.5. To the value of β, represented by ***k***, was assigned 1, 5, 10 and 30, illustrating negligible to significant ductility.

A generic design curve ω***i***α***j***β***k*** is a dimensionless N-M envelope curve, built from a set of analysis with DOCROS from N_{min} (maximum compressive force) and its corresponding maximum moment up to N_{max} (maximum tensile force) and its corresponding moment. In this process an increment of 100 kN for N was adopted. The generated data is plotted on dimensionless force (v) and dimensionless moment (μ), being calculated as

$$v = N/bdf_{ccp} \tag{4a}$$

$$\mu = M/bd^2 f_{ccp} \tag{4b}$$

In the generated v-μ curves v is assumed positive for compressive loads. The design values illustrated in Table 1 and 2 were used in the constitutive model of concrete and steel, respectively. In Table 1 ε_{ccp} is the concrete strain at peak compressive stress.

Table 1: Mechanical properties of the concrete used in constitutive model.

f_{ccp} (MPa)	ε_{ccp} (mm/mm)	E_c (GPa)	f_{ctc} (MPa)	f_{ctr} (MPa)	ε_{ctc} (mm/mm)	ε_{ctr} (mm/mm)	ε_{ctu} (mm/mm)
20.0	2.0×10^{-3}	29.0	1.33	αf_{ctc}	4.59×10^{-5}	$\beta\varepsilon_{ctc}$	2.0×10^{-3}

Table 2: Mechanical properties of the reinforcing bar used in the constitutive model.

f_{sy} (MPa)	ε_{sy} (mm/mm)	f_{sh} (MPa)	ε_{sh} (mm/mm)	f_{su} (MPa)	ε_{su} (mm/mm)	E_s (GPa)
348.0	1.74×10^{-3}	348.5	5.0×10^{-3}	349.0	0.1	200.0

In Table 2 f_{sh} and f_{su} is the hardening stress and the ultimate stress, respectively, and ε_{sh} and ε_{su} are the corresponding strains. E_s and ε_{sy} represent the elasticity modulus and the yielding strain of reinforcing bar, respectively.

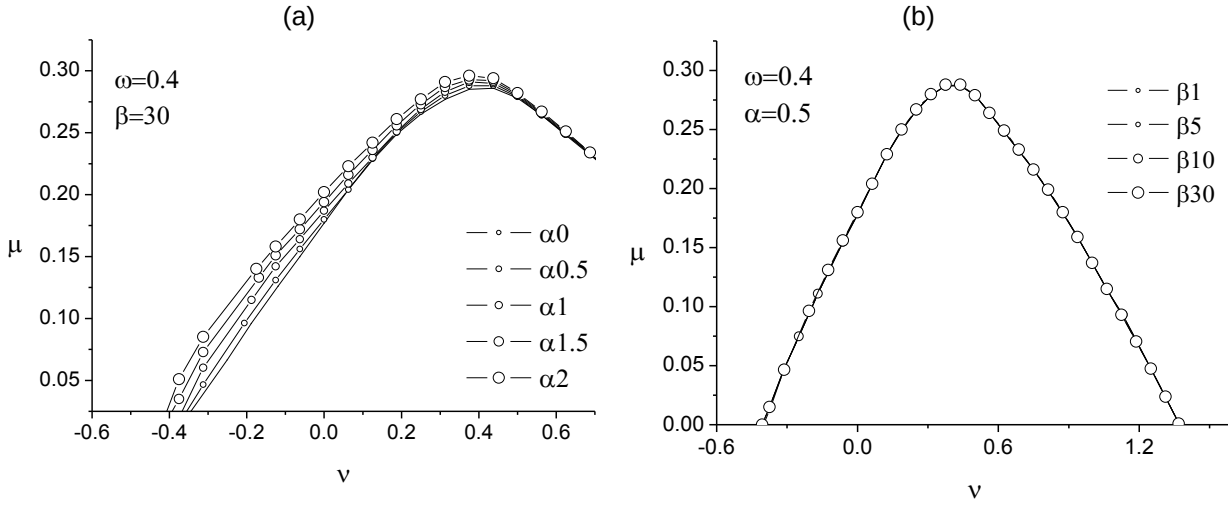

Figure 3: The *v-μ* diagrams by varying (a) *α* (b) *β.*

Figure 3(a) and Figure 3(b) illustrate a specific set of v-μ curve for varying *α* and *β*, respectively, for constant *ω*(0.4). These sets of Figure 3(a) and Figure 3(b) can be described by *ω0.4αjβ30 and* ω0.4*α*0.5***βk***, respectively. It should be noted that keeping all the parameters constant; change in *β* produces coinciding curves, while change in *α* generates slight variation in curves; as the increase in flexural capacity is dependent on tensile strength of concrete and not on ductility.

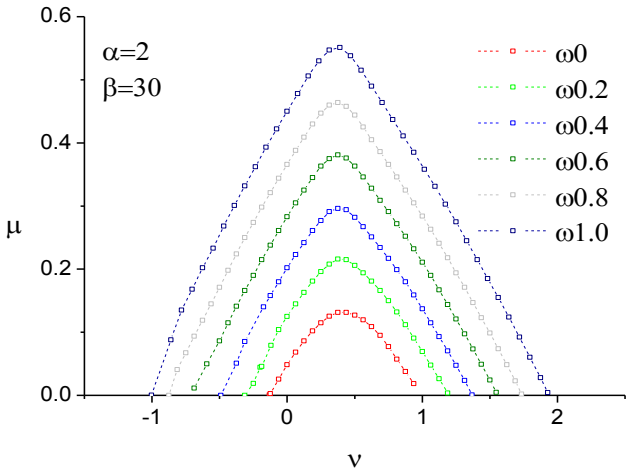

Figure 4: The *v-μ* diagrams by varying *ω*

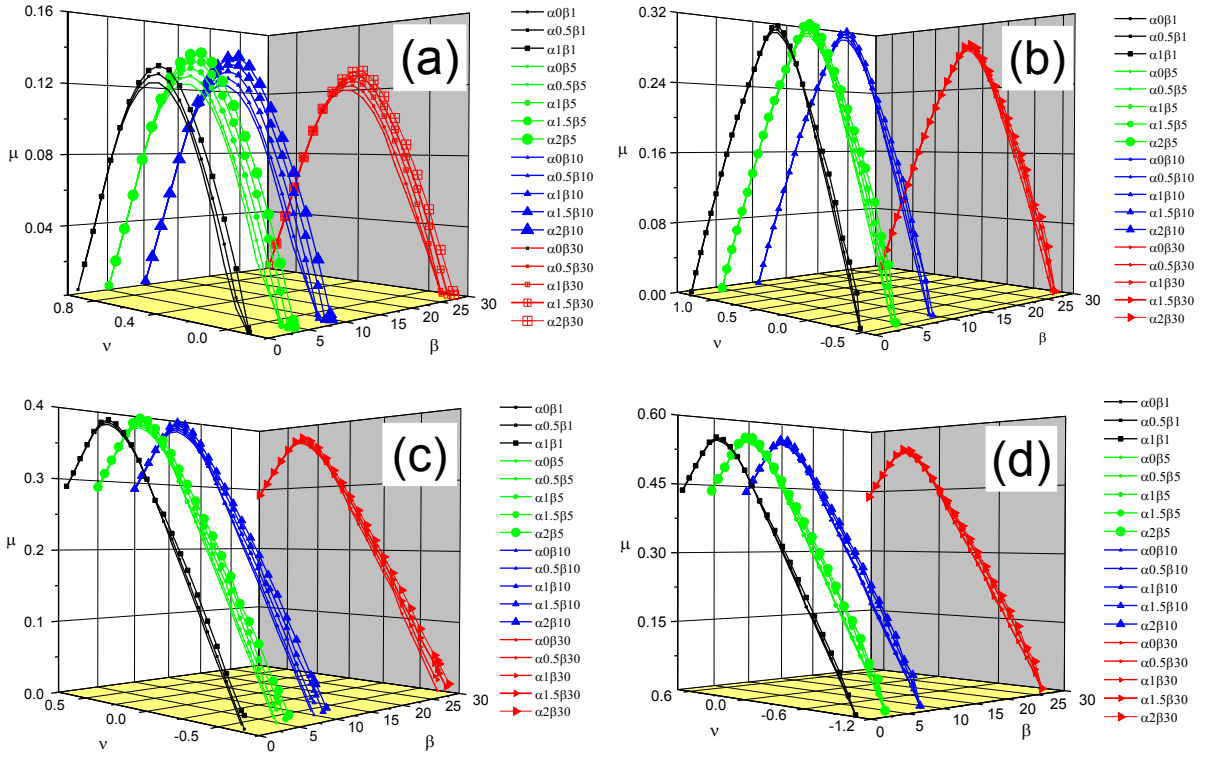

Figure 5: The *v-μ* diagrams for (a) *ω*=0 (b) *ω*=0.4 (c) *ω*=0.6 (d) *ω*=1.0.

The *v-μ* curve for varying *ω* from 0 to 1 with *α*=2 and *β*=30 is illustrated in Figure 4. With increase in reinforcement the bending and load carrying capacity of a section increases and as the analytical expressions for estimation of *M* and *N* remain same for these graphs, the generated curves are homologous in nature. Hence from design perspective, the favourable variation in diagrams is possible by varying either *α* or *ω*.

To present the curves in a more comprehensible way, v, μ and β are assumed as axes, and are plotted for every steel reinforcement ratio separately. The v-μ curves generated are illustrated in Figure 5 while the results for complete set of ω are described elsewhere [19]. To emphasize the effect of α for certain reinforcement ratios, Figure 5(c) and 5(d) represents a portion of v-μ curve with $v < 0.7$. After $v > 0.7$, the failure of section is governed by the compressive parameters; hence the effect of α is found to be insignificant.

In Figure 5 the size of the markers in the curves for each β is proportional to the α value. It is observed that for a definite β and ω, the flexural capacity increases with α. The favourable effect of α increases with the decrease of v and ω.

To illustrate the effect of α, the relationship $\Delta\mu \times 100/\mu_{RC}$ *versus* v is plotted in Figure 6 where differential dimensionless moment ($\Delta\mu$) is illustrated as:

$$\Delta\mu = \mu_{FRC} - \mu_{RC} \tag{5}$$

where μ_{FRC} and μ_{RC} represent dimensionless moment calculated for FRC and corresponding plain concrete section.

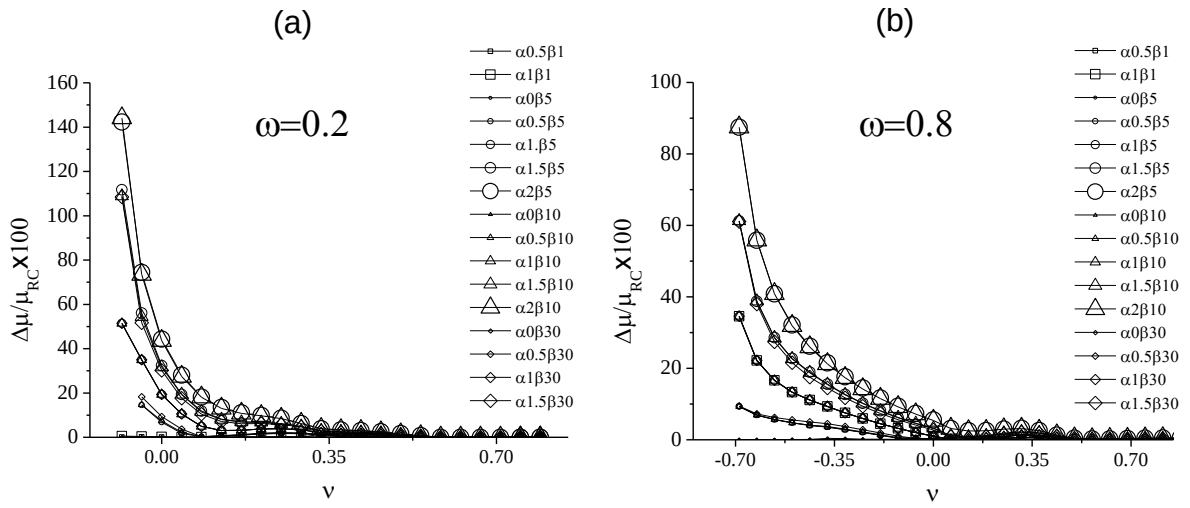

Figure 6: Percentage increase in dimensionless moment for (a) ω=0.2 (b) ω=0.8.

A $\alpha=0$ and $\beta=1$ represent the case of brittle failure. This situation can be assumed a benchmark similar to the plain concrete behaviour, for all ω. It should be noted that $\Delta\mu \times 100/\mu_{RC}$ increases with the decrease of v, which is attributed to the fact that by decreasing v, the M is calculated with increasing number of layers in tension, resulting in favourable effect of the FRC tensile parameters. In fact this figure shows the favourable effect of both α and β parameters on the flexural capacity of a cross section submitted to axial and bending moments. This reinforces that plain concrete when replaced by FRC, can increase the flexural capacity of cross-sections subjected to axial and bending moments. While for the same v, $\Delta\mu \times 100/\mu_{RC}$ is observed to have increase with increase in α. From Figure 6, it is inferred that the effect of ductility parameter β is insignificant; as μ is related to maximum moment, which does not depend on ductility.

5 DESIGN EXAMPLES

A surface represented in Figure 7(a) is generated by connecting a set of *v*-*μ* design curves by varying *β* and keeping *ω* and *α* constant. This representation shows clearly the benefits of *α* and *β* (specially the former one) on the flexural capacity of a cross section, but its use for design purposes is not simple. The design surface can be simplified by creating their contour map on a 2D *v*-*μ* representation, as shown in Figure 7(b), where design curves for *ω*=0 and *ω*=0.2 are plotted. Assuming a designer perspective, the graphic of Figure 7(b) is used to perform a design example.

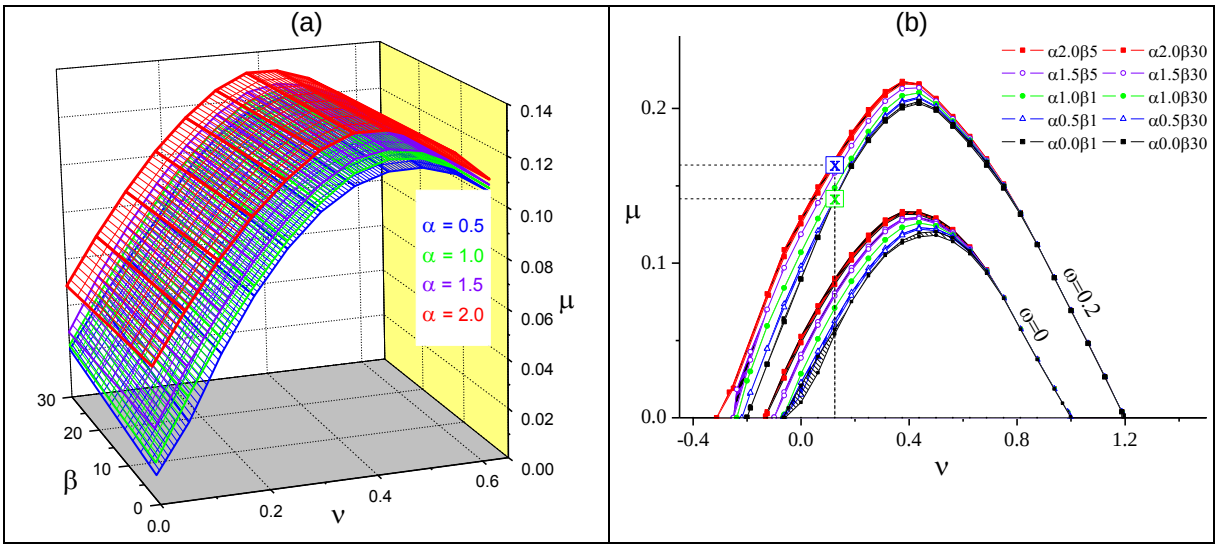

Figure 7: (a) Design surfaces for *ω*=0; and (b) Design curves for *ω*=0 and *ω*=0.2.

Consider an example with the cross section of 400 mm × 400 mm, with a reinforcement ratio of 0.2 and clear cover of 20 mm. For this section made of plain concrete, the hypothetical design load is 380 kN (*v* = 0.125) in compression and design moments is proposed. Assuming same reinforcement ratio and compressive load, the section is designed by FRC and the possible increase in moment capacity is discussed. From the Figure 7(b) the moment is found as 164.04 kN·m (*μ* = 0.142) on *α*0*β*1 (plain concrete) curve and illustrated by boxed **X** (in green colour). The maximum moment of *ω*=0.2 series is represented by boxed **X** (in blue colour, see Fig 7(b)) and found to be 193.78 kN·m, an increase of approximately 18%. The moments for the other cases lie in between the boxed **X**'s, (see in Fig 7(b)) and are presented in Table 4 with percentage increment with respect to plain concrete case (*ω*0.2*α*0*β*1). In case of SSFRC, the moment increase is insignificant, as the peak tensile strength in case of SSFRC is equal to the plain concrete. However, in case where plain concrete is completely replaced by SHFRC the increment in moment was significant. It is to be noted that the maximum moment of a section depends more on the tensile strength (or residual tensile strength, *α*) rather than ductility (or *β*), hence SHFRC can only yield favourable result.

Table 4. Increase in moment for strain hardening and strain softening FRC.

Strain softening material	Moment (kN·m)	Increase in Moment (%)	Strain hardening material	Moment (kN·m)	Increase in Moment (%)
$\alpha 0\beta 5$	164.04	0.002	$\alpha 1\beta j$*	172.20	4.974
$\alpha 0\beta 10$	164.04	0.002	$\alpha 1.5\beta 5$	183.45	11.831
$\alpha 0\beta 30$	164.14	0.063	$\alpha 1.5\beta 10$	182.69	11.371
$\alpha 0.5\beta 1$	164.40	0.222	$\alpha 1.5\beta 30$	181.18	10.450
$\alpha 0.5\beta 5$	164.40	0.221	$\alpha 2\beta 5$	193.78	18.130
$\alpha 0.5\beta 10$	164.43	0.237	$\alpha 2\beta 10$	193.68	18.072
$\alpha 0.5\beta 30$	164.52	0.295	$\alpha 2\beta 30$	189.34	15.472

* j = 1, 5, 10, 30

Consider another hypothetical example of a conventionally reinforced continuous shallow beam with three supports and spans of 5000 mm each in length. The geometry, support and reinforcement details of RC beam are illustrated in Figure 8. The beam design is simplified, and assumed to be composed of two types of cross-sections. The 1400mm length on each side of middle support is described by S_2-S'_2 section and the rest of beam is described by S_1-S'_1 section. The permissible deflection (δ) of the beam is $L/480$ (L=5000 mm is the span length of the beam) recommended by the ACI 318 (2004). The beam has the longitudinal reinforcement ratio (ρ) of 1.02% and 1.13% for sections S_1-S'_1 and S_2-S'_2, respectively, where

$$\rho = 100\,(A_s + A'_s) / bh \quad (6)$$

The beam was analysed for ultimate load carrying capacity by Femix, a finite element software developed with the collaboration of members of the Structural Composite research group of University of Minho. The analysis used Fibre model [19], in which the beam was divided in 22 Timoshenko beam elements of equal length, along the longitudinal direction. The cross section was divided in 40 concrete fibres, and each steel bar is assumed as an additional fibre. The design values of concrete and steel are described in Table 2 and 3, respectively. After applying dead load of 2.5kN/m^2, uniform distributed live load was applied until the displacement reached more than two times the permissible deflection. The force-deflection graphs are illustrated in figure 9, where force corresponds to total uniformly distributed load on each span, and deflection corresponds to mid-point of span (see point B in Figure 8).

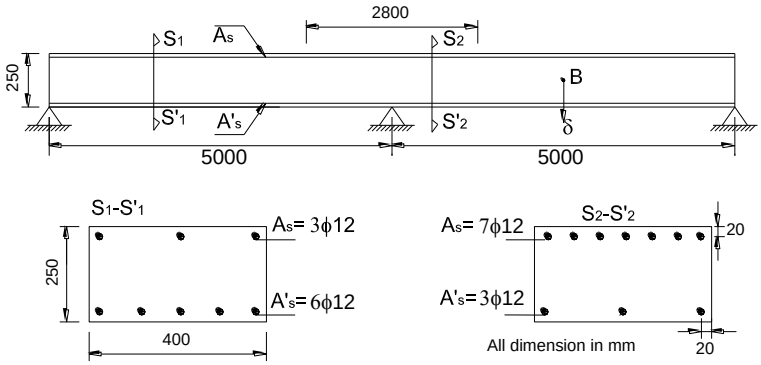

Figure 8: Beam and cross-sectional dimensions

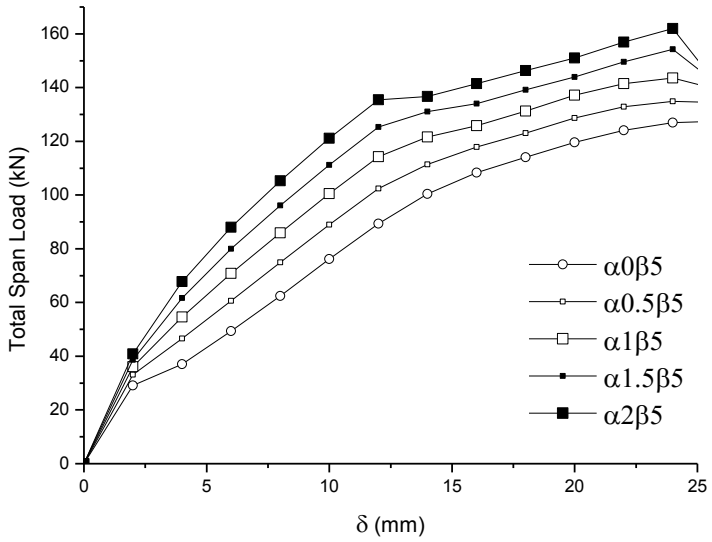

Figure 9: Force-deflection relationship of the continuous beam

From Figure 9, it can be seen that there was a substantial increment in load carrying capacity of beam. Table 5 presents the increment in terms of load percent for two deflection levels, δ and 2δ, for four different post-cracking performance of FRC. It can be concluded that the benefits in terms of load carrying capacity provided by a certain post-cracking performance of a FRC is higher than those at the cross section level. The benefits in term of load carrying capacity for serviceability and ultimate limit states increase with the degree of the statically indeterminacy of the structure.

Table 5. Increase in Span-Load for FRC continuous beams

FRC material	For δ deflection, increase in Span-Load (%)	For 2δ deflection, increase in Span-Load (%)
*α*0.5*β*5	16.62	7.5
*α*1*β*5	31.58	14.58
*α*1.5*β*5	45.36	20.14
*α*2*β*5	58.21	25.95

6 CONCLUSIONS

The present paper presented some design-curves of strain softening and strain hardening fibre reinforced concrete elements subjected to axial load and bending moments.

Due to advent of computation technology, the material properties can be used to precise value for finding the optimal solution, hence future design improvements are possible by improvement of material properties of concrete, like in case of FRC.

The shape of interaction curve depends on mechanical properties of concrete and steel, position of bars, reinforcement ratio and shape of the section. As FRC itself is composed of various small fibres, the design curves depend on mechanical properties of such fibres significantly.

The effect of *α* and *β* on the design a curve was noteworthy until the section failed in tension or was partially in tension during failure. The effect of *α* and *β* diminished for section failing in compression, because of the fact that neither the bending moment nor the axial load calculations are

governed by concrete tensile parameters. For a constant β, increasing in α has significant effect on v-μ curve. The response is attributed to possible higher strength even after cracking. While increasing in β and keeping α constant has insignificant effect.

The design example strengthens the fact that the FRC can be used as a partially replaceable material for reinforcement. The ductility parameter has insignificant effect on the maximum moment, but it should be noted that the structure failure is guided by ductility limits.

ACKNOWLEDGEMENTS

The first author acknowledges the support provided by FCT; grant number SFRH/BD/61677/2009. The study presented in this paper is a part of the research project titled “DURCOST - Innovation in reinforcing systems for sustainable pre-fabricated structures of higher durability and enhanced structural performance” with reference number of PTDC/ECM/105700/2008.

REFERENCES

[1] Romualdi, J.P., and Mandel, J.A., “Tensile Strength of Concrete Affected by Uniformly Distributed Closely Spaced Short Length of Wire Reinforcement”, ACI Journal, June 1964.
[2] Romualdi, J.P., “Two Phase Concrete and Steel Materials”, U.S. Patent No. 3,439,094, Feb. 25, 1969.
[3] Kelly, A., and Davis, G.J., “The Principles of Fiber Reinforcement of Metals”, Metallurgical Review, Vol. 10, No. 37, 1965.
[4] Majumdar, A.J., and Ryder, J.F., “Glass Fiber Reinforcement of Cement Products”, Glass Technology, Vol. 9, No. 3, June 1968, pp. 78−84.
[5] Majumdar, A.J., “Determining Bond Strength in Fiber Reinforced Composites”, Magazine of Concrete Research, Vol. 20, Dec. 1968.
[6] Aveston, J., Cooper, G.A., and Kelly, A., “Single and Multiple Fracture”, in Properties of Fiber Composites, Proceedings of Conference of the National Physical Laboratory, Guildford, U.K., IPC Science and Technology Press, 1971.
[7] Kelly, A., “Reinforcement of Structural Materials by Long Strong Fibers”, ASM Symposium,Boston, May 1972.
[8] Shah, S.P., Ranjan, R.V., “Fiber Reinforced Concrete Properties”, ACI Journal, Vol. 68, No. 2, Feb. 1971, pp. 126-135.
[9] Kelly, A., “Reinforcement of Structural Materials by Long Strong Fibers”, ASM Symposium, Boston, May 1972.
[10] Swamy, R.N., Editor, “Testing and Test Methods of Fiber Cement Composites”, RILEM Symposium Proceedings, Sheffield, The Construction Press, England, 1978, 545 pages.
[11] Neville, A., Editor, Proceedings of the RILEM International Symposium on Fiber Reinforced Cement and Concrete, London, September, 1975.
[12] Kasparkiewicsz, J., discussion, in Proceedings of RILEM Symposium on Testing and Test Methods of Fiber Cement Composites, Edited by N. Swamy, The Construction Press, England, 1978, pp. 493−495
[13] Naaman, A.E., and Shah, S.P., “Fracture and Multiple Cracking of Cementitious Composites”, in Fracture Mechanics Applied to Brittle Materials, ASTM STP 678, Part II, S.W. Frieman, Editor, 1979, 183-201.
[14] Naaman, A.E., and Reinhardt, H.W., “Proposed Classification of FRC Composites Based on their Tensile Response”, Materials and Structures, Vol. 39, page 547−555, 2006. Also, Proceedings of symposium honoring S. Mindess, N. Banthia, Editor, University of British Columbia, Canada, August 2005. Electronic proceedings, 13 pages.
[15] Parra-Montesinos, G.J. “High-Performance Fiber Reinforced Cement Composites: A New Alternative for Seismic Design of Structures”, ACI Structural Journal, 102(5), 2005, pp 668-675.

[16] Shah, S.P., Kuder, K.G. and Mu, B., “Fiber reinforced cement-based composites: a forty year odyssey”, Proceedings of the Sixth International Rilem Symposium, Varenna-Italy, 1 (2004) 3-30.
[17] Chang G.A., Mander J.B. “Seismic energy based fatigue damage analysis of bridge columns: Part I-Evaluation of seismic capacity”, Report No. NCEER-94-0006. 1994, 164 pp.
[18] Soranakom C, Mobasher B. “Closed form solutions for flexural response of fiber reinforced concrete beams”, Journal of Engineering Mechanics, V. 133, No 8, 2007, pp. 933–941.
[19] Varma R, “Modelling the cyclic behaviour of FRP strengthened RC structures”, Phd Thesis. Civil Engineering Department, University of Minho, 2012 (in press).
[20] ACI Committee 318, “Building code requirements for structural concrete and Commentary (ACI 318-04)”, Reported by committee 318, American Concrete Institute, Detroit, 351 pp., 2004.